Evolution of permeability in a natural fracture: Significant role of pressure solution

Hideaki Yasuhara and Derek Elsworth

Department of Energy and Geo-Environmental Engineering and Energy Institute, Pennsylvania State University, University Park, Pennsylvania, USA

Amir Polak

Department of Civil and Environmental Engineering, Technion-Israel Institute of Technology, Haifa, Israel

Received 30 June 2003; revised 27 October 2003; accepted 18 November 2003; published 13 March 2004.

[1] A mechanistic model is presented to describe closure of a fracture mediated by pressure solution; closure controls permeability reduction and incorporates the serial processes of dissolution at contacting asperities, interfacial diffusion, and precipitation at the free face of fractures. These processes progress over a representative contacting asperity and define compaction at the macroscopic level, together with evolving changes in solute concentration for arbitrarily open or closed systems for prescribed ranges of driving effective stresses, equilibrium fluid and rock temperatures, and fluid flow rates. Measured fracture surface profiles are applied to define simple relations between fracture wall contact area ratio and fracture aperture that represents the irreversible alteration of the fracture surface geometry as compaction proceeds. Comparisons with experimental measurements of aperture reduction conducted on a natural fracture in novaculite [*Polak et al.*, 2003] show good agreement if the unknown magnitude of microscopic asperity contact area is increased over the nominal fracture contact area. Predictions of silica concentration slightly underestimate the experimental results even for elevated microscopic contact areas and may result from the unaccounted contribution of free face dissolution. For the modest temperatures (20–150°C) and short duration (900 hours) of the test, pressure solution is demonstrated to be the dominant mechanism contributing to both compaction and permeability reduction, despite net dissolution and removal of mineral mass. Pressure solution results in an 80% reduction in fracture aperture from 12 μm, in contrast to a ~10 nm contribution by precipitation, even for the case of a closed system. For the considered dissolution-dominated system, fracture closure rates are shown to scale roughly linearly with stress increase and exponentially with temperature increase, taking between days and decades for closure to reach completion. *INDEX TERMS:* 5104 Physical Properties of Rocks: Fracture and flow; 5120 Physical Properties of Rocks: Plasticity, diffusion, and creep; 5139 Physical Properties of Rocks: Transport properties; 8045 Structural Geology: Role of fluids; 8160 Tectonophysics: Rheology—general; *KEYWORDS:* permeability, pressure solution, fracture

Citation: Yasuhara, H., D. Elsworth, and A. Polak (2004), Evolution of permeability in a natural fracture: Significant role of pressure solution, *J. Geophys. Res.*, *109*, B03204, doi:10.1029/2003JB002663.

1. Introduction

[2] The evolution of the mechanical and transport properties of rocks containing cracks at a variety of scales is strongly influenced by both the mechanical effects of crack formation, dilation, and closure, and their interaction with chemical effects of stress-mediated dissolution and precipitation. These effects are apparent for fractures at a variety of scales, from microcracks [e.g., *Tenthorey et al.*, 2003] to faults [*Tadokoro and Ando*, 2002], and control important processes including those of diagenesis, of strength gain on faults, of evolving pressure solution, of the development of reservoir seals, and of the evolution of flow pathways [*Durham et al.*, 2001; *Morrow et al.*, 2001].

[3] Data constraining the role of these chemical and mechanical interactions in fractures are sparse but are available at elevated temperatures (>300°C) in granite [*Moore et al.*, 1994], and at lower temperatures (50–150°C) in tuff [*Lin et al.*, 1997]. These are augmented by results for available composite aggregates of quartz [*Elias and Hajash*, 1992], halite [*Gratier*, 1993], calcite [*Zhang et al.*, 1994] and albite [*Hajash et al.*, 1998], at moderate temperatures (23–150°C), and the same material suites at elevated temperatures and pressures [e.g., *Zoback and Byerlee*, 1975; *Siddiqi et al.*, 2001]. The limited studies on fractures [*Moore et al.*, 1994; *Lin et al.*, 1997; *Durham et al.*, 2001; *Polak et al.*, 2003] suggest an increased sensitiv-

0148-0227/04/2003JB002663$09.00

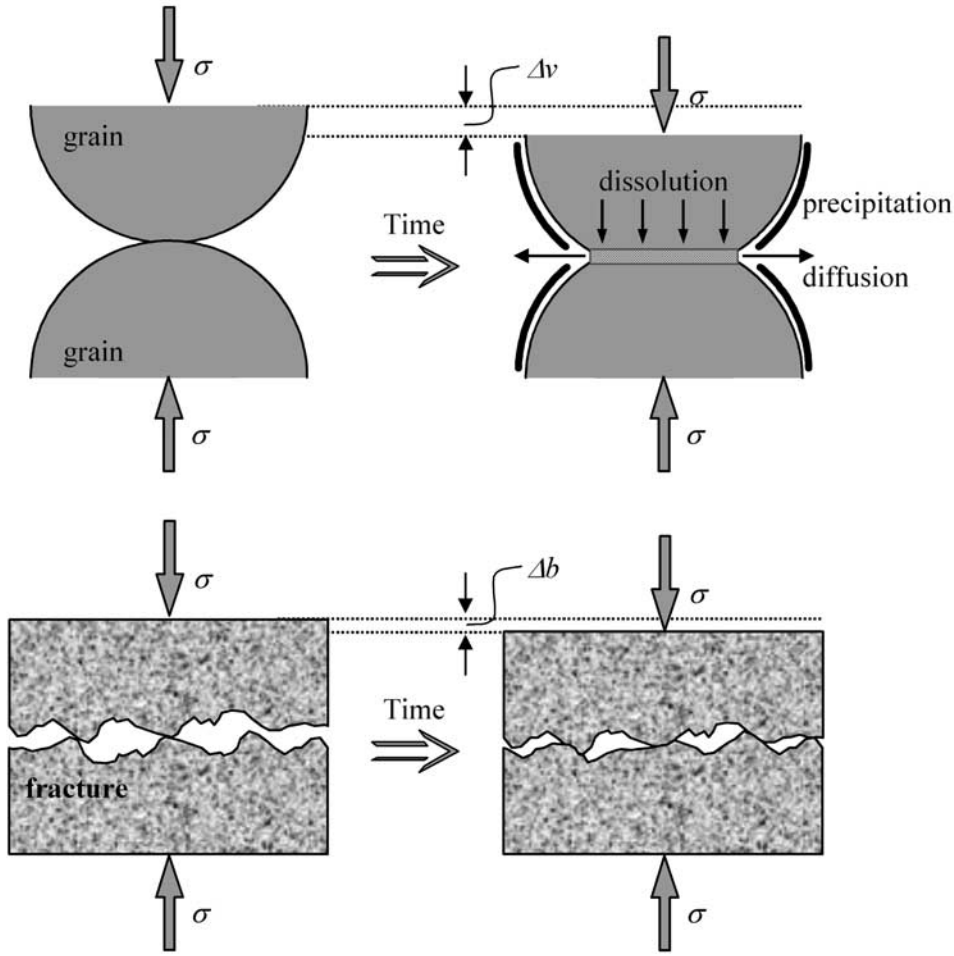

Figure 1. Schematic of pressure solution for twin contacting grains comprising an aggregate and fractured rock comprising a discontinuity. At the contacts the mineral dissolves due to high localized stresses, and dissolved mass diffuses from the interface into the pore space. Finally, precipitation occurs on the free faces of the pore walls.

ity of their transport properties to thermal, hydraulic, mechanical, and chemical processes, as compared to porous medium flows. This is apparent even at temperatures as low as 100°C, where the mobile dissolved species is silica, the test duration is of the order of a month [*Elias and Hajash*, 1992; *Lin et al.*, 1997], and where permeability may be reduced by a factor of 10^2 [*Polak et al.*, 2003].

[4] Apparent from these experimental data are the competing roles of processes that increase pore or flaw connectivity (including dilatant shear, microcracking, thermal cracking and focused dissolution) and those that destroy or counteract the evolution of pore interconnectivity (including shear and hydrostatic compaction, fracture healing, dislocation creep, and pressure solution prompted by water-film and free face diffusion). The sense of permeability change is controlled by the dominant processes; this is, in turn, largely controlled by the evolving conditions of effective stress, and temperature in the sample, and species concentrations within the effusing fluid.

[5] In this work we focus on the changes in transport parameters that result when a fracture is subjected to pressure solution by circulating hydrothermal fluids. The emphasis is in defining the processes that control the rates of pressure solution that consequently influence fracture aperture, and in turn control transport properties. The phenomenon of pressure solution is well defined for granular aggregates [*Weyl*, 1959; *Coble*, 1963; *Rutter*, 1976; *Raj*, 1982; *Tada et al.*, 1987] and represents a dominant mechanism for deformation and compaction within the upper earth crust [*Palciauskas and Domenico*, 1989; *Stephenson et al.*, 1992]. The process involves the serial processes of dissolution at highly stressed mineral contacts, the diffusive transport of dissolved mass along the contact boundaries, and ultimately the precipitation of mineral mass on available free faces. For granular aggregates, this process is defined schematically in Figure 1, together with the analogous process for the contacting asperities of a fracture. In this work we develop a model for porosity reduction in a natural fracture that honors the observations recovered from carefully constrained laboratory experiments on a stressed natural fracture in novaculite [*Polak et al.*, 2003]. This model accommodates the thermodynamics of pressure solution [e.g., *Shimizu*, 1995; *Paterson*, 1995; *Revil*, 1999, 2001], and yields changes in transport parameters as a natural consequence of following spatial changes in aperture that evolve with the mixed processes of dissolution and

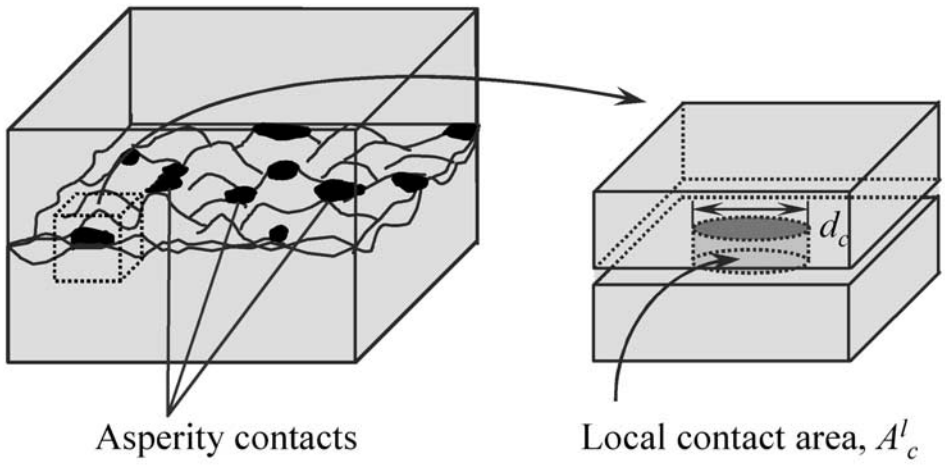

Figure 2. Idealized representation of the asperity contact condition. (right) A representative contact area, A_c^l, representing (left) the area of each asperity in contact and considered circular in shape, of diameter, d_c.

precipitation, mediated by local measures of stress and temperature dependence.

2. Conceptual Model

[6] A mechanistic model is presented to describe the stress- and dissolution-dependent closure of a fracture in rock that contributes to both changes in permeability and to an increase in strength. The fracture is idealized as two rough surfaces held apart by bridging asperities, as illustrated in Figure 1, with the gaping fracture represented by a capillary model. This geometry is directly analogous to that for a compacting granular aggregate [*Yasuhara et al.*, 2003] where stresses at grain contacts mobilize mineral mass that is transported along the intergranular boundary by a water film, and is then released into the pore void for later precipitation to the void walls or advection out of the system. Analogously, within the fracture, dissolved mineral mass is diffused along the water film contact between the asperities and effused into the fracture cavity, where it may either precipitate to seal the fracture or be advected from the system. These processes are described in the following.

2.1. Mechanistic Compaction Model of Fracture Mediated by Pressure Solution

[7] Pressure solution within a fracture incorporates the three serial processes: dissolution at asperity contacts, diffusion along the interfacial water film, and precipitation at the pore walls. First, dissolution at the asperity contacts provides a source of mass into the fracture cavity via diffusion along the asperity interface. This flux is driven by the gradient in chemical potential between the highly stressed portions of the contacting fracture and the less stressed site of the fracture wall. Dissolution is most conveniently defined in terms of a dissolution mass flux, dM_{diss}/dt, the rate of addition of dissolved mass into solution at the interface, given as [*Yasuhara et al.*, 2003]

$$\frac{dM_{\mathrm{diss}}}{dt} = \frac{3\pi V_m^2(\sigma_a - \sigma_c)k_+\rho_g d_c^2}{4RT}, \tag{1}$$

where V_m is molar volume of the solid (2.27×10^{-5} m^3 mol^{-1} for quartz), σ_a is the disjoining pressure [e.g., *Heidug*, 1995] equal to the amount by which the pressure acting at grain-to-grain contacts exceeds the hydrostatic pore pressure, k_+ is the dissolution rate constant of the solid, ρ_g is the grain density (2650 kg m^{-3} for quartz), d_c is the diameter of the asperity contact, R is the gas constant, T is the temperature of the system, and σ_c is the critical stress, which defines stress state where the compaction of grain aggregate will effectively halt [*Yasuhara et al.*, 2003]. This stress is determined by considering the energy balance under applied stress and temperature conditions, given by (*Revil* [1999], modified from *Stephenson et al.* [1992])

$$\sigma_c = \frac{E_m\left(1 - \frac{T}{T_m}\right)}{4V_m}, \tag{2}$$

where E_m and T_m are the heat and temperature of fusion, respectively (E_m = 8.57 kJ mol^{-1}, T_m = 1883 K for quartz).

[8] The local asperity-contact stress drives the process of mineral dissolution, and is amplified over the magnitude of the macroscopic stress by the ratio of tributary area to the local contact area. This average contact area ratio may be determined by defining a representative contact surrounded by an appropriate tributary area for the macroscopic stress (Figure 2). The average tributary area can be defined as the total surface area of the fracture, divided by the number of aperture contacts between fracture walls; these are macroscopic areas. Within this tributary area, the local (macroscopic) contact area, A_c^l, the diameter of the contact area, d_c, are defined as

$$d_c = \sqrt{\frac{4A_c^l}{\pi}}. \tag{3}$$

For uniaxial compaction, the normal forces acting on the tributary area and the contacting asperity balance, yielding the stress applied at the contact area, σ_a, as

$$\sigma_{\mathrm{eff}}A_t^l = \sigma_a A_c^l \Rightarrow \sigma_a = \sigma_{\mathrm{eff}}\frac{A_t^l}{A_c^l}, \tag{4}$$

where σ_{eff} is the average macroscopic effective stress and A_t^l is the average tributary area. The average contact area ratio, A_c^l/A_t^l, is assumed equivalent to the ratio of the summed local contact areas to the total fracture area, and defined as R_c.

[9] Second, on the basis of Fick's first law and integrating it with respect to a circular contact of radius r in the range $a \leq r \leq d_c/2$, diffusion along the asperity contact area is defined in terms of the diffusive mass flux, dM_{diff}/dt, as [*Yasuhara et al.*, 2003]

$$\frac{dM_{\text{diff}}}{dt} = \frac{2\pi\omega D_b}{\ln(d_c/2a)}\left(C_{\text{int}} - C_{\text{pore}}\right), \tag{5}$$

where ω is the thickness of the water film trapped at the interface, D_b is the diffusion coefficient, and $(C_{\text{int}})_{x=a}$ and $(C_{\text{pore}})_{x=d_c/2}$ are mineral concentrations in the interface fluid and pore space, respectively.

[10] Finally, precipitation of solute to the free faces of the fracture wall is described using the precipitation rate constant of quartz [*Canals and Meunier*, 1995; *Renard et al.*, 1997] and defined in terms of the precipitation mass flux, dM_{prec}/dt. This defines the rate of deposition of solute from the pore space onto the grain surfaces, as [*Yasuhara et al.*, 2003]

$$\frac{dM_{\text{prec}}}{dt} = V_p \frac{A}{M} k_- \left(C_{\text{pore}} - C_{\text{eq}}\right), \tag{6}$$

where V_p is the volume of the fracture void (for a parallel sided fracture this volume is the product of mean aperture and fracture area), k_- is the precipitation rate constant of the dissolved mineral, and C_{eq} is the equilibrium solubility of the dissolved mineral. A is the relative fracture surface area, and M is the relative mass of the fluid, which are dimensionless quantities defined by *Rimstidt and Barnes* [1980].

[11] The diffusion coefficient D_b, dissolution rate constant k_+, and precipitation rate constant k_- of quartz in equations (1), (5), and (6) have all Arrhenius-type dependence with temperature, given by

$$D_b = D_0 \exp(-E_D/RT), \tag{7}$$

$$k_+ = k_+^0 \exp(-E_{k+}/RT), \tag{8}$$

$$k_- = k_-^0 \exp(-E_{k-}/RT). \tag{9}$$

Appropriate magnitudes are selected for these constants defining the temperature dependence as $D_0 = 5.2 \times 10^{-8}$ m^2 s^{-1} and $E_D = 13.5$ kJ mol^{-1} [*Revil*, 1999], $k_+^0 = 1.59$ mol m^2 s^{-1} and $E_{k+} = 71.3$ kJ mol^{-1} [*Dove and Crerar*, 1990], and $k_-^0 = 0.196$ s^{-1} and $E_k^- = 49.8$ kJ mol^{-1} [*Rimstidt and Barnes*, 1980].

[12] For any applied stress and temperature condition, the concentration of the material in the fracture strongly influences the compactive process of fracture closure. The concentrations at the interface between the asperities and that in the fracture void may be defined [*Yasuhara et al.*, 2003] for both the open and the closed system as

$$\begin{pmatrix} C_{\text{int}} \\ C_{\text{pore}} \end{pmatrix}_{t+\Delta t} = \begin{bmatrix} D_1 + V_p/4\Delta t & -D_1 \\ -D_1 & D_1 + D_2 + V_p/2\Delta t \end{bmatrix}^{-1} \cdot \left[\begin{pmatrix} dM_{\text{diss}}/dt \\ D_2 C_{\text{eq}} \end{pmatrix}_{t+\Delta t} + \frac{1}{4\Delta t} \begin{bmatrix} V_p & 0 \\ 0 & 2V_p \end{bmatrix} \begin{pmatrix} C_{\text{int}} \\ C_{\text{pore}} \end{pmatrix}_t \right], \tag{10}$$

where

$$D_1 = \frac{2\pi\varpi D_b}{\ln(d_c/2a)}, \; D_2 = V_p \frac{A}{M} k_-, \tag{11}$$

and Δt denotes the time step.

2.2. Relation Between Contact Area and Aperture

[13] Closure rates of a fracture under applied stress and temperature conditions are controlled by the interaction of the serial processes of dissolution, diffusion, and precipitation. These processes irreversibly alter the geometry of the fracture surfaces and require that the initial fracture surface geometry is defined a priori. Profile data are necessary to define the relation between contact area and aperture, although data defining this relation are rare, despite the availability of proposed methods to quantify such relations [e.g., *Stesky and Hannan*, 1987; *Scavia*, 1999; *Gentier et al.*, 2000]. Consequently, a simplified, but physically viable, relation between fracture aperture and contact area is developed in this study.

[14] The topography of a rough fracture surface may be represented as a Gaussian distribution, given by

$$f(h) = \frac{1}{\sqrt{2\pi\sigma_h^2}} \exp\left[-\frac{(h - \langle h \rangle)^2}{2\sigma_h^2}\right], \tag{12}$$

where h is the elevation of the fracture surface, σ_h^2 is the variance, and $\langle h \rangle$ is the statistical average. The cumulative distribution function, which gives the probability that a variate will assume a value $\leq h$, is then the integral of the Gaussian function:

$$F(h) = \int_{-\infty}^{h} f(h')dh' = \frac{1}{2}\left[1 + \text{erf}\left(\frac{h - \langle h \rangle}{\sqrt{2\sigma_h^2}}\right)\right], \tag{13}$$

where erf is the error function. The aperture, b, of a fracture is the separation between the upper and lower rough surfaces. When the upper rough surface overrides and interpenetrates the lower surface, the mean aperture, $\langle b \rangle$, decreases with a concomitant increase in the contact area. If the two contacting surfaces exhibit a Gaussian distribution, the relation between aperture and contact area may be expressed as the cumulative distribution function similar to equation (13), as illustrated in Figure 3.

[15] Profile data from a fracture (Figure 4) are used to further constrain the relationship between aperture and contact area. The rough surface of the fracture is measured through laser profiling with vertical resolution of $\sim$1 μm on a rectangular lateral grid of $\sim$0.5 mm, as illustrated in Figure 4. The measured distribution of surface elevation is Gaussian. To obtain the relation between aperture and contact area, a replicated upper fracture surface is overlain, and the upper and lower surfaces are laterally offset by 0.5 mm [see, e.g., *Kishida et al.*, 2001; *Yasuhara et al.*, 2001]. Figure 5 depicts the relation between mean aperture, $\langle b \rangle$, and contact area ratio, R_c. The contact area ratio of this contacting fracture is merely defined by the ratio of the number of equally spaced profile points representing interpenetrated surfaces to the total number of measurement

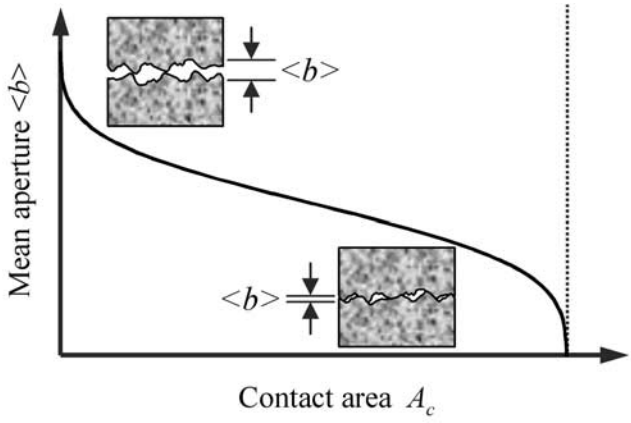

Figure 3. Relation between mean aperture and contact area of fracture. The relation is defined by the integral of the Gaussian distribution.

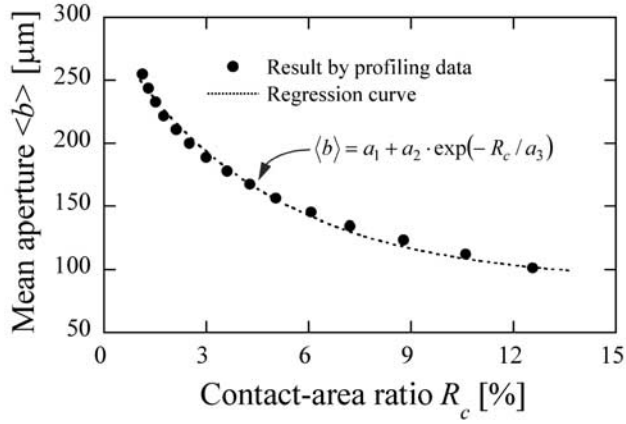

Figure 5. Relation between mean aperture and contact area ratio. Circles represent the profiling data, and dashed line is the regression curve $\langle b \rangle = a_1 + a_2 \exp(-R_c/a_3)$, where a_1 = 90.0, a_2 = 160.0, a_3 = 4.46, and the correlation coefficient, $R > 0.99$.

points. This relation is approximated by the regression curve, given by

$$\langle b \rangle = a_1 + a_2 \exp(-R_c/a_3), \tag{14}$$

where $\langle b \rangle$ is the mean aperture, R_c is the contact area ratio, and a_i (i = 1, 2, 3) is a constant. This regression curve is adopted as a straightforward and representative relation between fracture contact area and aperture to define the phenomenology of fracture sealing by pressure solution.

2.3. Overall Computational Procedure

[16] The three processes of dissolution, diffusion, and precipitation are combined to define the progress of aperture reduction of the fracture with time. In the initial condition, a small representative contact area is set with the initial aperture of the fracture. The relation between contact area and aperture in the representative elemental domain follows equation (14). An effective stress is applied, as amplified by the tributary geometry, and during time step Δt, appropriate magnitudes of mass dissolution, diffusion, and precipitation are simultaneously evaluated from equations (1), (5), and (6), respectively. Physically, the dissolved mass evaluated from equation (1) is supplied to the interface, and domain shortening, i.e., aperture reduction, proceeds as this mass passes along the interface by diffusion, as defined by equation (5). From the known magnitude of the diffusing mass, the updated contact area and aperture are calculated using the relation of equation (14) (the integration of equation (14) represents the removed volume, and its volume is matched by the diffused volume). A portion of the mass removed to the pore fluid may be deposited to the free surface of the fracture (equation (6)) and an additional reduction in aperture results. This deposition is controlled by the relative concentration differential between the pore fluid solution and the equilibrium concentration of that fluid. Concurrently, mineral concentrations in the interface

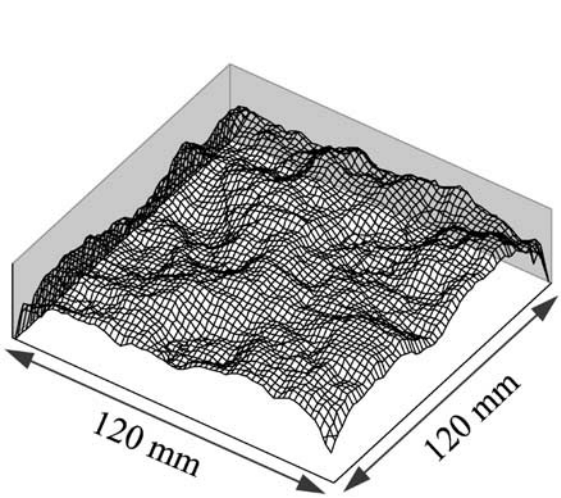

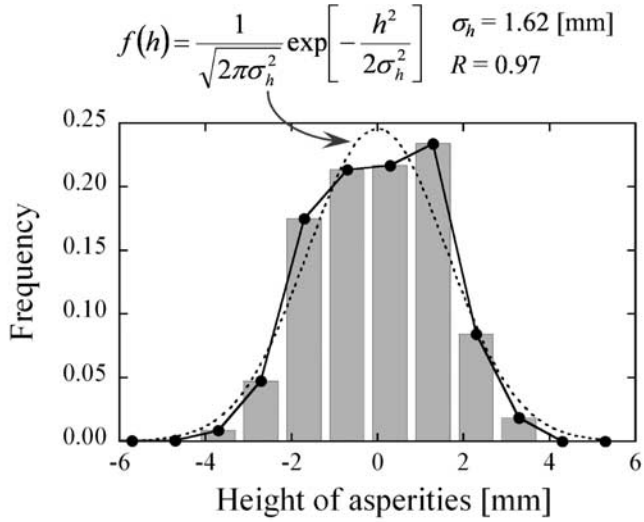

Figure 4. Oblique view of fracture profiling data and distribution of asperity heights. A null elevation represents the mean height of the fracture. Dashed line is an approximate Gaussian distribution.

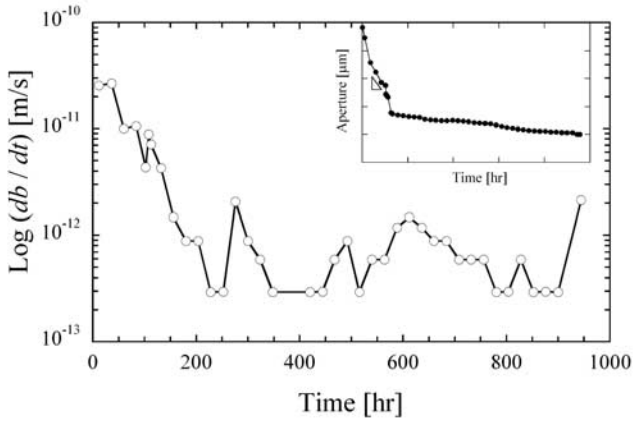

Figure 6. Rate of aperture reduction, *db*/*dt*, obtained from the experimental data of aperture change with time [*Polak et al.*, 2003].

fluid and the fluid in the fracture void fluid are updated utilizing equation (10). The solution procedure is repeated until the system reaches equilibrium, as the asperity contact area grows, and the driving asperity contact stress is correspondingly reduced.

3. Comparisons With Experimental Measurements

[17] The mechanistic model developed previously may be applied to describe the time-dependent reduction in aperture that results from the stressing of a natural fracture [*Polak et al.*, 2003]. Flow-through experiments have been conducted on a natural fracture of Arkansas novaculite, which has low porosity of <1%, a uniform grain size of the order of 1–6 μm, and quartz content of >99.5% [*Lee et al.*, 1991], at an average effective stress of 2.73 MPa and at temperatures of 20°C, 80°C, 120°C, and 150°C with the relatively high flow rates of 8.33×10^{-9}, 1.59×10^{-8}, 6.67×10^{-9}, and 3.75×10^{-9} m^3 s^{-1}, respectively [*Polak et al.*, 2003]. Changes in hydraulic aperture over the 900 hour test are evaluated from measurements of flow rate and pressure drop. The experimental measurements of aperture reduction showed an initial drop from ~12.5 to 9.0 μm at 20°C. This reduction likely results from the minor crushing of asperities and interstitial propping grains, with these processes dominating over the effect of pressure solution. A slow monotonic reduction in the fracture aperture was observed as the temperature was elevated sequentially to 80°C, 120°C, and 150°C. Aperture reductions for these three successive increases in temperature were ~3, 2, and 1 μm, respectively. Changes in silica concentration were measured during the first one hundred hours of the test, and used to constrain the influence of effective stresses and temperatures on compaction behavior and mineral dissolution.

3.1. Lumped Parameter Model Comparisons

[18] The dominant role of dissolution at contacting asperities has been examined in terms of the rate of aperture reduction, *db*/*dt* [*Polak et al.*, 2003], recorded from flow-through tests where independent estimates of fracture aperture are derived from the effusing fluid and mineral flux. Hydraulically measured aperture reduction rates, *db*/*dt*, are in the range 2.5×10^{-11} to 2.5×10^{-13} m s^{-1} as shown in Figure 6. The hydraulically measured rates may be augmented by estimates from mineral mass efflux, where an assumption is made regarding the contact area ratio, R_c, as

$$\frac{db}{dt} = \frac{QC_{\text{pore}}}{R_c A_f \rho_g}, \tag{15}$$

where A_f is the total fracture area ($A_f = 2.36 \times 10^{-3}$ m^2). By varying the unmeasured fractional contact area in the range of 5 to 30%, the rates of aperture reduction, *db*/*dt*, may be determined from the average recorded silica concentration, C_{pore}, of 0.77 ppm and measured flow rates, Q, of 1.59×10^{-8}, 6.67×10^{-9}, and 3.75×10^{-9} m^3 s^{-1} at 80°C, 120°C, and 150°C, respectively. These estimates, in the range of 10^{-10} to 10^{-12} m s^{-1}, are slightly higher than those recovered from the hydraulic measurements shown in Figure 7. This mismatch may result either from an unaccounted contribution of free face dissolution sourced from the fracture wall, or from an underestimate of assumed fracture contact area, commonly limited to ~30%. Free face dissolution may be active, since silica concentration in the pore fluid is much lower than the silica solubility (~30, 80, and 150 ppm at 80°C, 120°C, and 150°C, respectively). Alternatively, contact areas beyond commonly accepted magnitudes of ~30% are also feasible, given the progress of thermal annealing operative in the test, driven by pressure solution. The presence of a larger contact area than the expected one most consistently explains the mismatch between interpretations of the hydraulic and mass transport data.

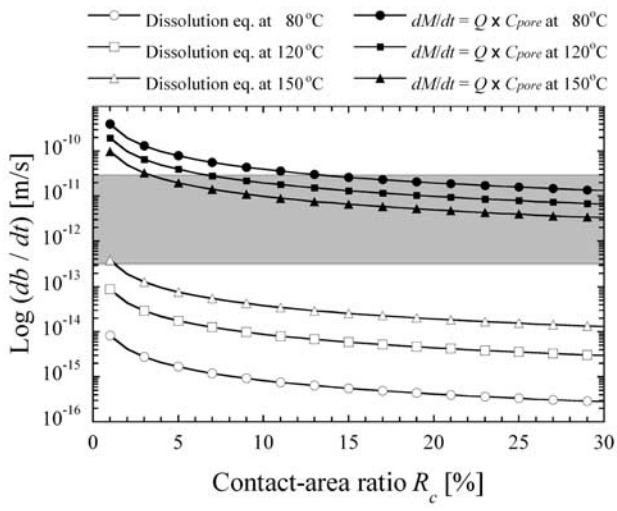

Figure 7. Comparison of the relation between rate of aperture reduction, *db*/*dt* and contact area ratio. Shaded area represents the range of rate of aperture reduction, *db*/*dt*, obtained from experimental data [*Polak et al.*, 2003] (Figure 9). Solid circles, squares, and triangles represent predictions by equation (16) at 80°C, 120°C, and 150°C, respectively. Open circles, squares, and triangles represent predictions by equation (18) at 80°C, 120°C, and 150°C, respectively.

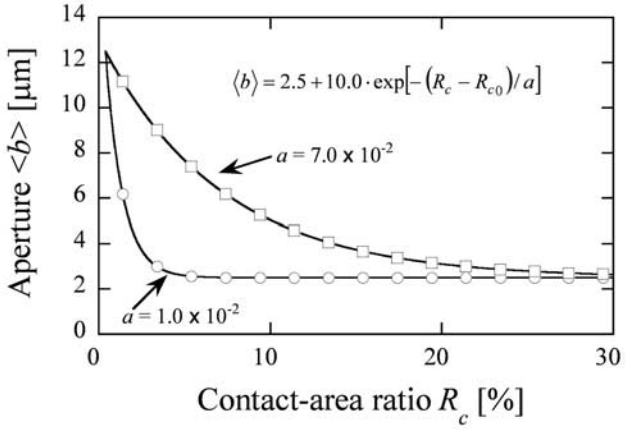

Figure 8. Relation between aperture and contact area ratio. Two different relations are set. The curve with open circles shows a sharper reduction of aperture with an increase of contact area than the relation represented by the open squares.

[19] In this work the dissolution mass flux, dM_{diss}/dt, is defined as in equation (1), and the anticipated rates of aperture reduction, db/dt, may be independently recovered from the predicted rates of asperity dissolution, under stress, given by

$$\frac{db}{dt} = \frac{dM_{\text{diss}}}{dt}\frac{1}{A_c^l \rho_g}. \tag{16}$$

Substituting the mass flux that results from dissolution under the asperity contacts (equation (1)) via the defined contact area, $A_c^l = \pi d_c^2/4$, into equation (16), results in an aperture change rate of

$$\frac{db}{dt} = \frac{3V_m^2(\sigma_a - \sigma_c)k_+}{RT}. \tag{17}$$

Stresses applied at contact area, σ_a, are much larger than the critical stresses, σ_c, when the compacting process is far from the equilibrium state, and equation (17) may be modified by neglecting the term of the critical stress, σ_c, given by

$$\frac{db}{dt} \approx \frac{3V_m^2\sigma_a k_+}{RT} = \frac{1}{R_c}\cdot\frac{3V_m^2\sigma_{\text{eff}}k_+}{RT}. \tag{18}$$

The rates of aperture reduction, db/dt, are predicted at 80°C, 120°C, and 150°C for unmeasured contact areas in the range of 1–30% as shown in Figure 7. As apparent from Figure 7, aperture closure rates predicted by equation (18) are 1–3 orders of magnitude smaller than those obtained by experimental measurements (in the range 2.5×10^{-11} to 2.5×10^{-13} m s^{-1}).

3.2. Numerical Model Comparisons

[20] The behavior of the fracture is followed using the model introduced in section 2. This model follows the change in mechanical aperture with time, rather than the hydraulic aperture, which is recovered from the flow-through experimental results via the "cubic law" [*Piggott and Elsworth*, 1993; *Polak et al.*, 2003]. Despite this minor inconsistency, mechanical and hydraulic apertures are assumed approximately equivalent [*Piggott and Elsworth*, 1993], as is reasonable to a first-order estimate. Throughout the test duration, silica concentrations within the fluid remains very low (of the order of <1 ppm), confirming that precipitation remains inactive within the fracture throughout the 900 hours duration of the experiment (silica solubility is in the range 32–155 ppm at 80–150°C [*Fournier and Potter*, 1982]). The low silica concentrations highlight the potential for the activation of free face dissolution; this effect is not significant in this particular example, and its analysis is not included. To follow the experimental measurements of rates of aperture reduction without the effects of precipitation, we modify equation (10) by substituting $D_2 = 0$ and the concentration in the interface at contact area is given by

$$C_{\text{int}}|_{t+\Delta t} = \frac{(D_1 + V_p/2\Delta t)\left[(dM_{\text{diss}}/dt) + (V_p/4\Delta T)C_{\text{int}}|_t\right] + (D_1 V_p/2\Delta t)C_{\text{pore}}|_t}{(D_1 + V_p/4\Delta t)(D_1 + V_p/2\Delta t) - D_1^2}, \tag{19}$$

where

$$D_1 = \frac{2\pi\varpi D_b}{\ln(d_c/2a)}. \tag{20}$$

Concentration in the fluid is obtained straightforwardly from the relation between dissolved mass of quartz transported into the fluid and the flow rates, given by

$$C_{\text{pore}} = \frac{1}{Q}\frac{dM_{\text{diff}}}{dt}, \tag{21}$$

where Q denotes the flow rate.

[21] Throughout the duration of the experiment, the fracture aperture changes from ~12.5 μm to ~2.5 μm, and approaches an equilibrium closure at intermediate temperatures during the experiment [*Polak et al.*, 2003]. Correspondingly, the initial aperture is set to 12.5 μm, and the relation between contact area and aperture is given by equation (14) as

$$\langle b \rangle = 2.5 + 10.0\exp[-(R_c - R_{c0})/a], \tag{22}$$

where R_{c0} is the initial contact area ratio, which is an arbitrary ratio chosen at the beginning of the analysis, with the fracture subsequently consolidating to an equilibrium closure. (Note that the initial value for R_{c0} of 1% contact area ratio is set in the calculations, and predictions of aperture reduction are never conditioned by R_{c0} even for 0.1% or 0.5% contact area ratio as initial.) The process of aperture reduction is strongly influenced by this aperture to contact area relation, and parameterizations are utilized to follow the experimental measurements, as depicted in Figure 8.

[22] We initiate our calculations from a temperature of 80°C, where the effects of pressure solution are anticipated significant. The initial silica concentration is evaluated from the total mass removed in the first 36 hours, as the initial fracture aperture falls to 9.0 μm (based on equation (22)), for a known total volume of flow at 20°C. During the

Table 1. Parameters Used to Represent the Experimental Results

Effective Stress σ_{eff}, MPa	Diffusion Path Width ω, nm	Temperature T, °C	Diffusion Coefficient D_b, $m^2\ s^{-1}$	Dissolution Rate Constant k_+, $mol\ m^{-2}\ s^{-1}$	Critical Stress σ_c, MPa
2.73	4.0	80	5.24×10^{-10}	4.52×10^{-11}	76.7
		120	8.36×10^{-10}	5.35×10^{-10}	74.7
		150	1.12×10^{-9}	2.51×10^{-9}	73.2

experiments, two sharp reductions in aperture result from the unanticipated shutdown of the water injection pump. These occurrences are followed by resetting the aperture according to the closure recorded in the experiment: the contact area ratio and concentrations are updated using equation (22).

[23] Parameters utilized in the calculations are summarized in Table 1. Predicted rates of aperture reduction are shown in Figure 9 together with the data measured through the experiments. As apparent in Figure 9, the predictions underestimate the actual closure, which is likely due to underestimation of surface area where the interface dissolution proceeds. The macroscopic contact area, is not the same as the microscopic area of the contact plane that participates in the dissolution reaction, but is indexed to it. In order to obtain more realistic predictions, the fracture surface areas should be evaluated microscopically. Therefore we introduce a roughness factor, f_r [*Murphy and Helgeson*, 1989], which is the ratio of the true (microscopic) surface area over the apparent (microscopic) surface area. Considering the microscopic surface area, dissolution and precipitation mass flux is magnified by the roughness factors, f_r, and equations (1) and (6) are modified as

$$\frac{dM_{\mathrm{diss}}}{dt} = f_r \frac{3\pi V_m^2 (\sigma_a - \sigma_c) k_+ \rho_g d_c^2}{4RT} \tag{23}$$

$$\frac{dM_{\mathrm{prec}}}{dt} = f_r V_p \frac{A}{M} k_- \left(C_{\mathrm{pore}} - C_{\mathrm{eq}}\right). \tag{24}$$

To closely match the aperture reduction obtained in the experiments, the roughness factors, f_r, are increased by factors of 300 (80°C), 40 (120°C), and 40 (150°C) and of 3000 (80°C), 300 (120°C), and 300 (150°C) for $a = 1.0 \times 10^{-2}$ and $a = 7.0 \times 10^{-2}$, respectively. The predictions of aperture reduction obtained using the augmented roughness factors, f_r, are in good agreement with the actual data, as shown in Figure 9, while the predictions of silica concentration (Figure 10) still underestimate the experimental measurements. This underprediction may easily result from the unaccounted contribution of free face dissolution, which may dominate the aqueous concentration response. Equilibrium saturations of silica are in the range 30–150 ppm at temperatures of 80–150°C, 2 orders of magnitude above those measured. A small contribution of dissolved mass from a proportionately small area of contacting asperities, results in a disproportionate contribution in fracture closure, as inferred by the rate, db/dt, represented in equation (15). The multipliers applied to the roughness factors are relatively large but are premised on the contrasting and undefined magnitudes of the fracture surface areas obtained at "macroscopic" and "microscopic" levels. Accordingly, with unmodulated constants, this model will underestimate the dissolution rate, and this is consistent with comparison results of aperture closure rates, db/dt, as shown in Figure 7. (Note that aperture closure rates obtained by equation (18) are compatible with those

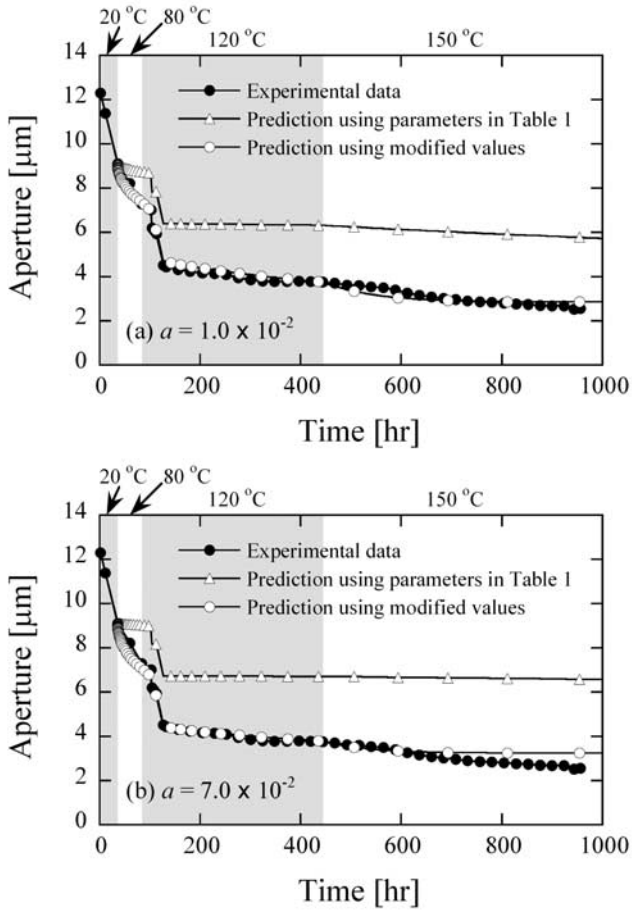

Figure 9. Comparison of aperture reduction with time between experimental data of *Polak et al.* [2003] and predictions of the current model. (a) For $a = 1.0 \times 10^{-2}$ in equation (22), open triangles represent the prediction using parameters shown in Table 1, and open circles represent the prediction using modified values with f_r = 300.0, 40.0, and 40.0 for T = 80°C, 120°C, and 150°C, respectively. (b) For $a = 7.0 \times 10^{-2}$ in equation (22), open triangles represent the prediction using parameters shown in Table 1, and open squares represent the prediction using modified values with f_r = 3000.0, 300.0, and 300.0 for T = 80°C, 120°C, and 150°C, respectively.

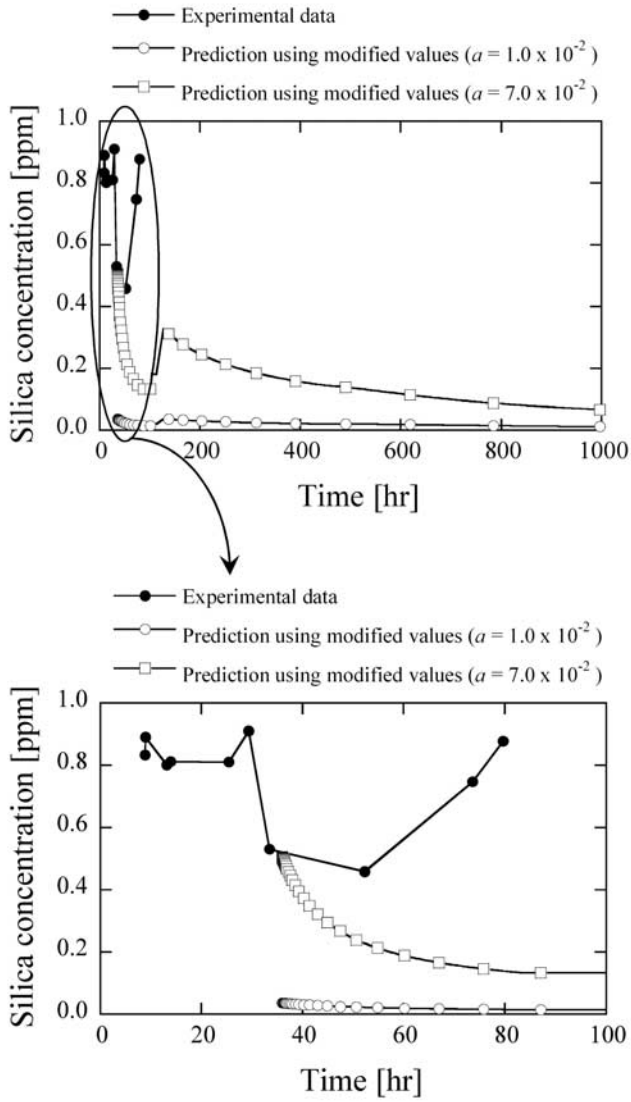

Figure 10. Comparison of change of silica concentration with time between experimental data of *Polak et al.* [2003] and predictions of our model. For $a = 1.0 \times 10^{-2}$ in equation (22), open circles represent the prediction using modified values with f_r = 300.0, 40.0, and 40.0 for T = 80°C, 120°C, and 150°C, respectively. For $a = 7.0 \times 10^{-2}$ in equation (22), open squares represent the prediction using modified values with f_r = 3000.0, 300.0, and 300.0 for T = 80°C, 120°C, and 150°C, respectively.

determined from the hydraulic measurements (db/dt in the range 2.5×10^{-11} to 2.5×10^{-13} m s^{-1}) when the roughness factors are increased by 3 orders of magnitude for 80°C and 2 orders of magnitude for 120°C and 150°C, similar to the multipliers applied to replicate the experimental results; that is, f_r, is applied by multipliers of 300 (80°C), 40 (120°C), and 40 (150°C) and of 3000 (80°C), 300 (120°C), and 300 (150°C) for $a = 1.0 \times 10^{-2}$ and $a = 7.0 \times 10^{-2}$, respectively.) The multipliers on the roughness factors are larger at 80°C than the multipliers at either 120°C or 150°C. This is attributed to the observation that mechanical closure effects, such as the failure of contacting asperities, is dominant at 80°C rather than compaction mediated by mineral dissolution.

[24] Precipitation contributes crucially to the compaction processes through the potential to occlude the fracture void and to thereby add to the apparent reduction in transport aperture. This effect is a maximum for a closed system, where the captured silica is retained within the fracture void, and may be represented by the computational procedure described previously. Where the same roughness factors are used, as previously, the predictions of aperture changes for the closed system are insignificant. The total thickness of the precipitated layer is the order of ~10 nm. In practice, precipitation may localize close to its source at the asperity contact area, and result in a more significant impact on transport behavior, than if uniformly distributed over the fracture wall.

[25] Further consideration is given to the influence of system temperatures (80°C, 150°C, and 200°C) and applied effective stresses (2.73, 5.00, and 10.00 MPa) on the progress of fracture closure. For a fracture of identical contact area ratio to aperture relation ($a = 1.0 \times 10^{-2}$) to that considered previously, the reduction in aperture with time is followed in Figure 11. The appropriate parameters, congruent with those used previously, are summarized in Table 2. For the particular ranges of parameters, representative of a tight (initial aperture ~12 μm) fracture in quartz novaculite, strong dependencies on ambient stress and

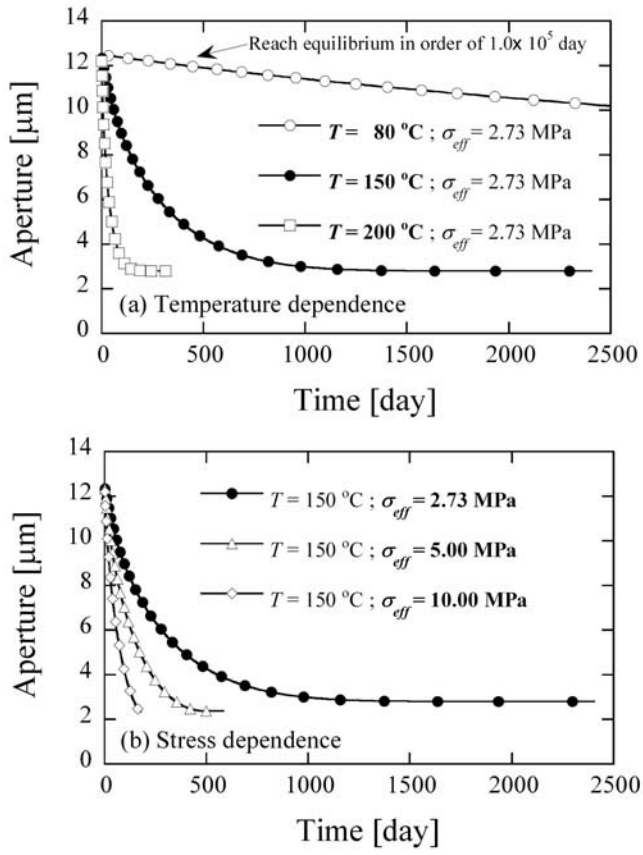

Figure 11. Predictions of aperture reduction in a fracture with time under various system conditions of (a) temperature and (b) effective stress.

Table 2. Parameters Used to Examine the Closure of a Fracture Under Effective Stresses in the Range 2–10 MPa and Temperature of 80–200°C[a]

Effective Stress σ_{eff}, MPa	Temperature T, °C	Diffusion Coefficient D_b, $m^2\ s^{-1}$	Dissolution Rate Constant k_+, mol $m^{-2}\ s^{-1}$	Precipitation Rate Constant, k_-, s^{-1}	Critical Stress σ_c, MPa
2.73	80	5.24×10^{-10}	4.52×10^{-11}	8.43×10^{-9}	76.7
5.00	150	1.12×10^{-9}	2.51×10^{-9}	1.42×10^{-7}	73.2
10.00	200	1.68×10^{-9}	2.14×10^{-8}	6.23×10^{-7}	70.7

[a]See Figure 11.

temperature are apparent. For these parameters, the role of precipitation is minor, with little influence on the compaction process (the contribution by precipitation is less than 1% of the total aperture reduction). Under constant effective stresses, the equilibrium aperture of the fracture asymptotes to the same closure for all temperatures. This is expected since the asymptotic behavior is controlled by the dual parameters of critical stress, σ_c, and equilibrium contact area. Critical stress is only slightly influenced by system temperature, and contact area will evolve similarly for a given contact area to aperture relation for the fracture. In this case, the closure from 12 to 2 μm over the period of the test results in a net reduction in permeability of over 2 orders of magnitude. For this particular case where precipitation has little influence, the influence of temperature is larger than that for stress. This results from the significant influence that the dissolution rate constant, k_+, exerted through the Arrhenius-type (exponential) dependence. Where effective stresses are increased under constant temperatures (Figure 11b), the rate dependence of closure is less pronounced. Doubling stresses, essentially doubles the closure rate, as anticipated in the linear stress dependency of the numerator of equation (1). Lower effective stresses result in slightly smaller levels of ultimate closure, as conditioned by the reduced contact area required to elevate stresses to equilibrium contact magnitudes, σ_c.

4. Conclusions

[26] A mechanistic model is developed to represent the processes of aperture change and related changes in permeability in a natural fracture that incorporates the significant role of pressure solution. This behavior is represented by the three serial processes of dissolution, diffusion, precipitation, that redistribute mineral mass from contacting asperities either to the fracture walls, or to the system exterior. The interaction of these processes at a representative contacting asperity allows the closure of a contacting fracture to be followed with time under arbitrary conditions of effective stress and temperature. A simple relation between fracture aperture and fracture contact area ratio is defined to represent the geometric modification of the fracture surfaces as compaction proceeds, and the fracture walls attempt to interpenetrate.

[27] The current model is capable of representing the compaction process, and changes in fracture aperture and mineral mass concentration in the effluent fluid may be followed with time. Predictions of the evolution in fracture aperture replicate experimental measurements, but aqueous concentrations of silica are underestimated, even with the inclusion of roughness factors to account for the mismatch between macroscopic and microscopic contact areas. This mismatch may result from a potentially dominant contribution of free face dissolution to aqueous concentrations in the silica-undersaturated permeant, relative to a mechanical response dominated by minor mass removal from limited areas of contact; fracture closure is amplified by a small asperity contact area. Rates of pressure solution are indexed by magnitudes of the roughness factors, modified in this work to accommodate unknown and unmeasured microscopic reactive surface areas that exist at fracture asperity contacts. The multipliers are significant but are premised on the contrasting and undefined magnitudes of the fracture surface areas obtained at macroscopic and microscopic levels. These magnitudes are consistent between comparisons in terms of the rates of aperture reduction, db/dt, between the experimental measurements and the predictions based on the dissolution mass flux that show nominal agreement with the thousandfold (80°C) and hundredfold (120°C and 150°C) roughness factors. For a closed system, predictions indicate the insignificant contributions of precipitation to the compaction processes through the potential to occlude the fracture void. In practice, precipitation may localize close to its source at the contacting asperities, and result in a more significant impact on transport behavior, than if uniformly distributed over the fracture wall.

[28] The rate of aperture reduction increases as temperature and applied stress increase. For the dissolution-dominated system examined here, the dependency of aperture reduction rate on stress is roughly linear: doubling the effective stress roughly doubles the closure rate. However, the dependency on temperature is more pronounced due to the linkage of dissolution rate with its Arrhenius-type (exponential) dependence. Where evolving changes in contact area are ignored, the mass removal rate, scales roughly as

$$\frac{dM_{\text{diss}}}{dt} \propto \frac{k_+^0}{RT} \exp(-E_{k+}/RT)$$

(from equations (1) and (8)) and the overriding control on temperature is apparent. Durations for the completion of aperture reduction are reduced from a few centuries to approximately a year at temperatures in the range 80–200°C, and from a few years to a fraction of a year at effective stresses in range 3–10 MPa.

[29] Aperture reduction as the compaction proceeds may result in healing and related strength gain on fractures. This consideration is important in considering strength gain in reservoir rocks, and the development of sealing and healing on active faults. In this work simple relations between

fracture contact area and fracture aperture are defined, but quantitative evaluations for strength recovery are not considered. For this, further geometric constraints of two rough surfaces in contact are required.

[30] **Acknowledgments.** This work is a result of partial support under grants DOE-BES-DE-FG02-00ER15111 and DOE-DE-PS26-01NT41048. This support is gratefully acknowledged. The comments of two anonymous reviewers contributed to the quality of the final manuscript.

References

Canals, M., and J. D. Meunier (1995), A model for porosity reduction in quartzite reservoirs by quartz cementation, *Geochim. Cosmochim. Acta*, *59*, 699–709.

Coble, R. L. (1963), A model for boundary diffusion controlled creep in polycrystalline materials, *J. Appl. Phys.*, *34*, 1679–1682.

Dove, P. M., and D. A. Crerar (1990), Kinetics of quartz dissolution in electrolyte solutions using a hydrothermal mixed flow reactor, *Geochim. Cosmochim. Acta*, *54*, 955–969.

Durham, W. B., W. L. Bourcier, and E. A. Burton (2001), Direct observation of reactive flow in a single fracture, *Water Resour. Res.*, *37*, 1–12.

Elias, B. P., and A. Hajash (1992), Change in quartz solubility and porosity change due to effective stress: An experimental investigation of pressure solution, *Geology*, *20*, 451–454.

Fournier, R. O., and R. W. Potter II (1982), An equation correlating the solubility of quartz in water from 25°C to 900°C at pressure up to 10,000 bars, *Geochim. Cosmochim. Acta*, *46*, 1969–1973.

Gentier, S., J. Riss, G. Archmbault, R. Flamand, and D. Hopkins (2000), Influence of fracture geometry on shear behavior, *Int. J. Rock Mech. Min. Sci.*, *37*, 161–174.

Gratier, J. P. (1993), Experimental pressure solution of halite by an indenter technique, *Geophys. Res. Lett.*, *20*(15), 1647–1650.

Hajash, A., T. D. Carpenter, and T. A. Dewers (1998), Dissolution and time-dependent compaction of albite sand: Experiments at 100°C and 160°C in pH-buffered organic acids and distilled water, *Tectonophysics*, *295*, 93–115.

Heidug, W. K. (1995), Intergranular solid-fluid phase transformations under stress: The effect of surface forces, *J. Geophys. Res.*, *100*, 5931–5940.

Kishida, K., A. Adachi, and K. Tsuno (2001), Modeling of the shear behavior of rock joints under constant confining conditions, *Proc. U.S. Rock Mech. Symp.*, *38th*, 791–798.

Lee, V. W., S. J. Mackwell, and S. L. Brantley (1991), The effect of fluid chemistry on wetting textures in novaculite, *J. Geophys. Res.*, *96*, 10,023–10,037.

Lin, W., J. Roberts, W. Glassley, and D. Ruddle (1997), Fracture and matrix permeability at elevated temperatures, paper presented at Workshop on Significant Issues and Available Data, Near-Field/Altered-Zone Coupled Effects Expert Elicitation Project, U.S. Dep. of Energy, San Francisco, Calif., Nov.

Moore, D. E., D. A. Lockner, and J. D. Byerlee (1994), Reduction of permeability in granite at elevated temperatures, *Science*, *265*, 1558–1561.

Morrow, C. A., D. E. Moore, and D. A. Lockner (2001), Permeability reduction in granite under hydrothermal conditions, *J. Geophys. Res.*, *106*, 30,551–30,560.

Murphy, W. M., and H. C. Helgeson (1989), Thermodynamic and kinetic constraints on reaction rates among minerals and aqueous solutions. IV. Retrieval of rate constants and activation parameters for the hydrolysis of pyroxene, wollastonite, olivine, andalusite, quartz, and nepheline, *Am. J. Sci.*, *289*, 17–101.

Palciauskas, V. V., and P. A. Domenico (1989), Fluid pressures in deforming porous rocks, *Water Resour. Res.*, *25*, 203–213.

Paterson, M. S. (1995), A theory for granular flow accommodated by material transfer via an intergranular fluid, *Tectonophysics*, *245*, 135–151.

Piggott, A. R., and D. Elsworth (1993), Laboratory assessment of the equivalent apertures of a rock fracture, *Geophys. Res. Lett.*, *20*(13), 1387–1390.

Polak, A., D. Elsworth, H. Yasuhara, A. S. Grader, and P. M. Halleck (2003), Permeability reduction of a natural fracture under net dissolution by hydrothermal fluids, *Geophys. Res. Lett.*, *30*(20), 2020, doi:10.1029/2003GL017575.

Raj, R. (1982), Creep in polycrystalline aggregates by matter transport though a liquid phase, *J. Geophys. Res.*, *87*, 4731–4739.

Renard, F., P. Ortoleva, and J. P. Gratier (1997), Pressure solution in sandstones: Influence of clays and dependence on temperature and stress, *Tectonophysics*, *280*, 257–266.

Revil, A. (1999), Pervasive pressure-solution transfer: A poro-visco-plastic model, *Geophys. Res. Lett.*, *26*(2), 255–258.

Revil, A. (2001), Pervasive pressure solution transfer in a quartz sand, *J. Geophys. Res.*, *106*, 8665–8686.

Rimstidt, J. D., and H. L. Barnes (1980), The kinetics of silica-water reactions, *Geochim. Cosmochim. Acta*, *44*, 1683–1699.

Rutter, E. H. (1976), The kinetics of rock deformation by pressure solution, *Philos. Trans. R. Soc. London, Ser. A*, *283*, 203–219.

Scavia, F. R. C. (1999), Determination of contact areas in rock joints by X-ray computer tomography, *Int. J. Rock Mech. Min. Sci.*, *36*, 883–890.

Shimizu, I. (1995), Kinetics of pressure solution creep in quartz: Theoretical considerations, *Tectonophysics*, *245*, 121–134.

Siddiqi, G., B. Evans, G. Dresen, and D. Freund (2001), Effect of semi-brittle deformation on transport properties of calcite rocks, *J. Geophys. Res.*, *106*, 8665–8686.

Stephenson, L. P., W. J. Plumley, and V. V. Palciauskas (1992), A model for sandstone compaction by grain interpenetration, *J. Sediment. Petrol.*, *62*, 11–22.

Stesky, R. M., and S. S. Hannan (1987), Growth of contact area between rough surfaces under normal stress, *Geophys. Res. Lett.*, *14*, 550–553.

Tada, R., R. Maliva, and R. Siever (1987), Rate laws for water-assisted compaction and stress-induced water-rock interaction in sandstones, *Geochim. Cosmochim. Acta*, *51*, 2295–2301.

Tadokoro, K., and M. Ando (2002), Evidence for rapid fault healing derived from temporal changes in S wave splitting, *Geophys. Res. Lett.*, *29*(4), 1047, doi:10.1029/2001GL013644.

Tenthorey, E., S. F. Cox, and H. F. Todd (2003), Evolution of strength recovery and permeability during fluid-rock reaction in experimental fault zones, *Earth Planet. Sci. Lett.*, *206*, 161–172.

Weyl, P. K. (1959), Pressure solution and the force of crystallization—A phenomenological theory, *J. Geophys. Res.*, *64*, 2001–2025.

Yasuhara, H., K. Kishida, and T. Adachi (2001), Prediction of shear behavior of a single joint using profiling data (in Japanese), *Proc. Jpn. Rock Mech. Symp. Tokyo, 31st*, 161–165.

Yasuhara, H., D. Elsworth, and A. Polak (2003), A mechanistic model for compaction of granular aggregates moderated by pressure solution, *J. Geophys. Res.*, *108*(B11), 2530, doi:10.1029/2003JB002536.

Zhang, S., S. Cox, and M. Paterson, (1994), The influence of room temperature deformation on porosity and permeability in calcite aggregates, *J. Geophys. Res.*, *99*, 761–775.

Zoback, M., and J. Byerlee (1975), The effect of microcrack dilatancy on the permeability of Westerly Granite, *J. Geophys. Res.*, *80*, 752–755.

D. Elsworth and H. Yasuhara, Department of Energy and Geo-Environmental Engineering and Energy Institute, Pennsylvania State University, University Park, PA 16802, USA. (huy103@pau.edu)

A. Polak, Department of Civil and Environmental Engineering, Technion-Israel Institute of Technology, Haifa 32000, Israel.